

Clinical Validation of Angle-Independent Myocardial Elastography Using MRI Tagging

Wei-Ning Lee¹, Zhen Qian², Dimitris N. Metaxas² and Elisa E. Konofagou^{1,3}

¹Department of Biomedical Engineering, Columbia University, New York, NY, USA, ²Department of Biomedical Engineering, Rutgers University, Piscataway, NJ, USA, ³Department of Radiology, Columbia University, New York, NY, USA
ek2191@columbia.edu

Abstract— In this paper, two-dimensional angle-independent myocardial elastography (2DME) was employed in order to assess and image myocardial deformation (or, strains) in an entire left-ventricular view and was further validated against tagged Magnetic Resonance Imaging (tMRI) in normal as well as abnormal human subjects. Both RF ultrasound and tMRI frames were acquired in a 2D short-axis (SA) view at the papillary muscle level. In 2DME, in-plane (lateral and axial) incremental displacements (i.e., between two consecutive RF frames) were iteratively estimated using 1D cross-correlation and recorrelation techniques in a 2D search with a 1D matching kernel. The incremental displacements starting from end-diastole (ED) to end-systole (ES) were then accumulated to obtain cumulative systolic displacements. In tMRI, cardiac motion was obtained using a template-matching algorithm on a 2D grid-shaped mesh. The entire displacement distribution within the myocardium was obtained by a cubic B-spline-based method. In both 2DME and tMRI, 2D Lagrangian finite systolic strains were calculated from cumulative 2D displacements. Principal strains, which were angle-independent and less centroid dependent than polar (i.e., radial and circumferential) strains, were then computed from the 2D finite strains through our previously established strategy. Both qualitatively (or, full SA view) and quantitatively (or, temporal strain profiles), 2DME is shown capable of estimating myocardial deformation highly comparable to tMRI estimates in a clinical setting.

Keywords: *angle-independent; circumferential; cross-correlation; elastography; magnetic resonance imaging; myocardial; principal; radial; radio-frequency; recorrelation; strain; tagging.*

I. INTRODUCTION

Echocardiography has been widely used in the clinic owing to its higher temporal resolution, low cost, portability, familiarity to cardiologists and low patient exclusion rate. Abnormal myocardial deformation is a critical indicator of cardiac diseases, such as ischemia or infarction. Two-dimensional myocardial elastography (2DME), which is a radio-frequency (RF) based speckle tracking technique, has been evaluated regarding its feasibility of assessing normal myocardial deformation [1] and detecting abnormal myocardial function [2], due to ischemia or infarction, through estimation and imaging of the myocardial deformation during natural contraction of the myocardium. We have previously proposed a theoretical framework [3], which showed the excellent performance of 2DME in accurately estimating and imaging in-plane displacements and deformation (i.e., strains) in a full short-axis (SA) view using both an ultrasonic image formation

model and an established three-dimensional (3D) finite-element canine left ventricular model, in both normal and left-circumflex (LCx) ischemic cases. Not only was 2DME shown to accurately estimate the myocardial displacements and strains using that theoretical model, but it could also differentiate abnormal from normal cardiac muscles without beam-to-muscle angle (i.e., the orientation of the ultrasound transducer relative to the left ventricle) dependence based on polar (i.e., radial and circumferential) strain estimation [3].

Although the polar strains are independent of the beam-to-myocardium angle, they have been proven to be highly dependent on the manual centroid selection [4], further affecting the accuracy of differentiating the abnormal from normal cardiac muscles. In order to reduce the centroid dependence, an angle-independent and less centroid-dependent measure, namely the principal strain, has been proposed and evaluated based on the abovementioned theoretical framework in a separate study by our group [4, 5]. Angle-independent myocardial elastography, which integrated the estimation of 2D displacements, 2D strains, and principal strains, were thus employed in this paper.

In clinical applications, the assessment of myocardial deformation using cardiac tagged Magnetic Resonance Imaging (tMRI) [6, 7] is currently considered as the noninvasive gold standard. Several studies have compared the estimates from ultrasound with those from tMRI [8, 9]. Notomi et al. [8] and Helle-Valle et al. [9] have demonstrated that left ventricular torsion measured from B-mode-based speckle tracking methods is consistent with that from tMRI in short-axis (SA) views. In this paper, we focus on full SA depiction of in-plane myocardial deformation (i.e., strains) based on the RF-based, and therefore more precise, 2DME technique in a clinical setting in order to evaluate the myocardial strain estimates and validate them against the tMRI findings.

II. METHODS

A. High frame-rate ultrasound data acquisition

A clinical echocardiography ultrasound scanner (GE Vivid FiVe, GE Vingmed Ultrasound, Horten, Norway) with a phased array probe operating at 2.5 MHz was used to acquire cardiac ultrasound in-phase and quadrature (I/Q) data in 2D SA views at the papillary muscle level of normal and abnormal human left ventricles. The I/Q data were then upsampled to retrieve the RF signals. A frame-rate of 136 fps was achieved based on a novel electrocardiogram (ECG)-gated composite imaging, which assembled multiple small sector data into a

full-view echocardiogram and was implemented by our group [10]. Slightly different from the fully automated method [10], in this study, five or six sectors with a reduced field of view (FOV) were manually selected and combined off-line based on the spatial (i.e., depth and angle) and ECG information to reconstruct an entire SA echocardiograms at 136 fps using the GE system. RF data of each sector were acquired over three cardiac cycles. Each sector was acquired during separate breath-holds and free-hand scanning, and the total acquisition time was approximately six minutes.

B. MRI data acquisition

Tagged MR images were obtained on Philips Intera 1.5T scanner (Philips Medical Systems, Best, The Netherlands) equipped with a five-channel SENSE cardiac coil and Master gradients of strength 30 mT/m and slew rate 150 T/m/s. Multi-slice and multi-phase true SA tagged images were acquired under free-breathing with a combination of fast-field echo excitation and a multi-shot echo-planar readout (EPI-FFE) technique [11] (FOV=350 mm, TE=4 ms, TR=30, NSA=4, resolution acquired/reconstructed=192/256, flip angle =13 degrees, EPI factor=3 and full ECG gating scan duration=4.77 min). Two-dimensional grid tagging was performed, yielding a 9-mm, in-plane tag resolution. Six SA slices throughout the left ventricles were imaged, and the slice at the papillary muscle level was further used for this comparison study. The nominal frame rate of the MR tagging sequence was 33 fps.

The human subject study protocol was approved by the Institutional Review Board of Columbia University, and informed consent was obtained from all human subjects prior to scanning.

C. Two-dimensional myocardial elastography (2DME)

The two in-plane orthogonal displacement components (lateral and axial) were iteratively estimated on RF signals using one-dimensional (1D) cross-correlation and recorrelation in a 2D search [3]. The cross-correlation technique employed a 1D matching kernel of 7.7 mm and 80% overlap. The reference and comparison frames respectively contained the RF signals before and after deformation occurred. An 8:1 linear interpolation scheme between two adjacent original RF signal segments of the comparison frame within the 1D kernel was employed to improve the lateral resolution [12]. The maximal cross-correlated value yielded from the RF signal segment in the comparison frame was considered the best match with the RF signal segment in the reference frame. Cosine interpolation was then applied around this peak of the cross-correlation function for a more refined peak search [12].

The correction (or, recorrelation) in axial displacement estimation [3], was performed to reduce the decorrelation resulting from axial motion for more precise lateral displacement estimation. In 2DME, recorrelation was implemented by shifting RF signal segments according to the estimated axial displacement in the comparison frame, prior to the second lateral displacement estimation.

The incremental displacements were integrated to obtain the cumulative displacement that occurred from end-diastole (ED) to end-systole (ES). Appropriate registration for each pixel on two consecutive displacement images was performed

in order to further ensure that the cumulative displacement depicted the motion of the same tissue region.

D. Motion estimation from MRI tagging (tMRI)

Tagged MRI [6, 7] generates two perpendicular sets of equally spaced parallel tagging planes within the myocardium as temporary markers at end-diastole through spatial modulation of the magnetization. Imaging planes are perpendicular to the two sets of tagging planes so that the tags appear as dark grids on MR images and deform with the underlying myocardium during the cardiac cycle *in vivo*. This can yield detailed motion information of the myocardium.

In order to track the tagging grids and get the localized myocardial displacement and strain values, a template-based tracking algorithm on a 2D grid-shaped mesh was implemented to obtain the displacement vectors of the crossing points (or, nodes) on the tagging grids [13-16]. Each node on the mesh was tracked by calculating the similarity between templates, which were modeled using two tunable Gabor filters and the underlying images. The crossing points on the mesh were driven iteratively by forces from the neighboring image patches, whose texture patterns were the most similar to a reference template. The coordinates of the crossing points in a time sequence were further smoothed by a cubic spline function, and the displacements were thus calculated through subtraction. Finally, a cubic B-spline-based method was used to obtain the entire displacement distribution within the myocardium [17].

E. Angle-independent (or, principal) strain estimation

Cumulative 2D (i.e., lateral and axial) systolic Lagrangian finite strain was first derived from the cumulative 2D displacement to evaluate the systolic function *in vivo* [3]. Positive and negative 2D strains indicate tension and compression, respectively. In 2DME, a least-squares strain estimator (LSQSE) [18] with a kernel of 11.7 mm in both the lateral and axial directions was used in order to improve the elastographic signal-to-noise ratio (SNRe) in a strain image and to simultaneously achieve similar image resolutions between tMRI and 2DME for subsequent comparison.

Principal strains, which were angle-independent and less-centroid-dependent than polar strains, were then yielded by solving the eigenvalue/eigenvector problem for the abovementioned 2D finite strain [4, 5]. Two principal strain components were relevant to the two eigenvalues, and their principal axes corresponded to eigenvectors, which were further classified using a classification strategy to closely approximate the radial and circumferential directions [4, 5]. Note that the two principal strains were classified according to their angles between the principal and polar directions [4] and that the principal strains presented throughout this paper referred to classified principal strains.

F. Automatic contour tracking

Segmenting the myocardium from the neighboring tissue is essential in the depiction and detection of the extent of the pathological myocardium. The myocardial segmentation on the elastographic images throughout the entire cardiac cycle was performed and extended from 1D (i.e., axial) to 2D using an automated method [19]. The endo- and epi-cardial contours on

the initial echocardiogram (i.e., at ED) were manually traced with 20 points each as reference, while those for the rest of the frames were automatically segmented according to the estimated 2D displacement components.

III. RESULTS

A. A normal human left ventricle

The anterior, lateral, posterior and septal walls are indicated in the upper right, lower right, lower left, and upper left regions, respectively. Figure 1 shows the cumulative systolic lateral and axial strains estimated from tMRI ((a) and (c)) and 2DME ((b) and (d)). As expected for a normal left ventricle being imaged in an echocardiographic SA view, tension in the lateral direction appears in lateral and septal myocardial regions, and axial tension in the anterior and posterior walls. The cumulative systolic principal strains estimated from both imaging modalities are shown in Fig. 2, which shows myocardial thickening in (a) and (b) (i.e., positive 1st principal strain) and shortening in (c) and (d) (i.e., negative 2nd principal strain).

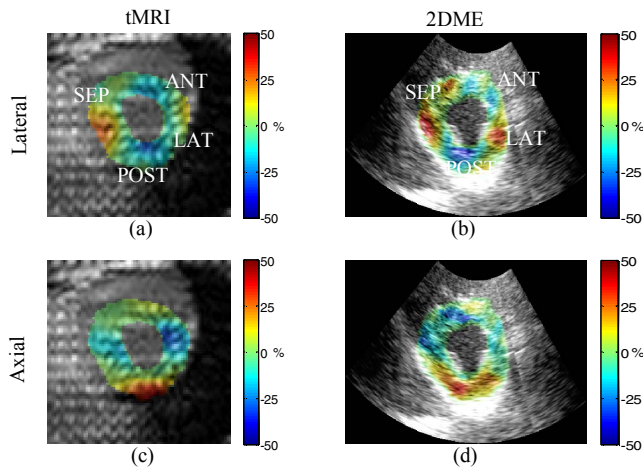


Fig. 1 Cumulative systolic 2D strains of a normal human left ventricle between ED and ES: (a) and (c) are the lateral and axial strains from tMRI, respectively; (b) and (d) are the lateral and axial strains from 2DME, respectively. All the strain images are acquired approximately at the papillary muscle level and shown at ES. (These figures should be received/printed in color.)

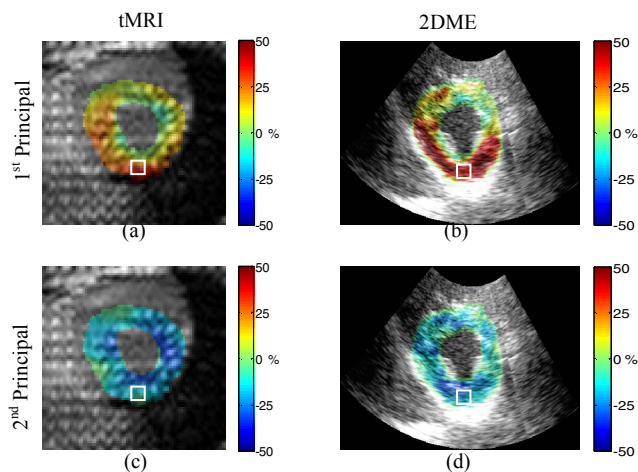


Fig. 2 Cumulative systolic principal strains of the same normal human left ventricle between ED and ES: (a) and (c) are the 1st and 2nd principal strains from tMRI, respectively; (b) and (d) are the 1st and 2nd principal strains from 2DME, respectively.

B. A reperfused human left ventricle

This human subject suffered a myocardial infarction caused by partial occlusion of the distal left anterior descending (LAD) coronary artery and subsequent motion abnormalities in both the septal and anterior walls. Figure 3 shows the estimated cumulative systolic 2D strains. Not only does the reperfused left ventricle (Fig. 3) show hypokinetic behavior in the post-infarcted (i.e., anterior and anteroseptal) region and hyperkinetics in the normal (i.e., lateral and lateral-posterior) wall region compared with the normal left ventricle (Fig. 1), but the 2D strain patterns of the reperfused one (Fig. 3) are highly asymmetric compared to those of the normal one (Fig. 1). The cumulative systolic 1st principal 2DME strain estimate (Fig. 4(b)) for the reperfused left ventricle shows myocardial thickening in the posterior and anterior-septal segment but not in the septum or anterior regions. On the contrary, the 1st principal tMRI strain (Fig. 4(a)) shows thickening throughout the entire myocardium with augmented thickening in the posterior wall but with reduced thickening in the other wall regions. The 2nd principal 2DME strain estimate (Fig. 4(d)) shows myocardial shortening in the posterior wall and slight stretching in the other regions, while the corresponding tMRI estimate (Fig. 4(c)) indicates slight stretching in the lateral, anterior and anterior-septal walls.

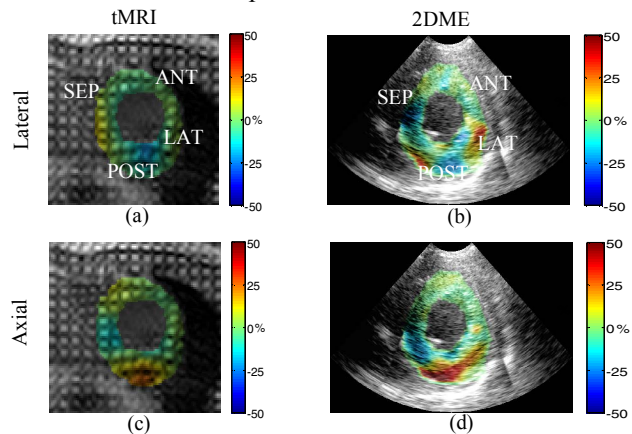


Fig. 3 Cumulative systolic 2D strains of a reperfused human left ventricle between ED and ES: (a) and (c) are the lateral and axial strains from tMRI, respectively; (b) and (d) are the lateral and axial strains from 2DME, respectively. All the strain images are acquired approximately at the papillary muscle level and shown at ES.

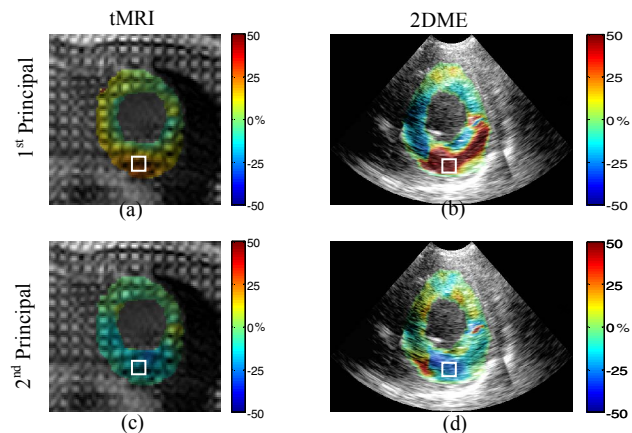


Fig. 4 Cumulative systolic principal strains of the same reperfused human left ventricle between ED and ES: (a) and (c) are the 1st and 2nd principal strains from tMRI, respectively; (b) and (d) are the 1st and 2nd principal strains from 2DME, respectively.

C. Temporal strain profiles

The temporal principal strain profiles for both normal and reperfused left ventricles during systole in a posterior wall region of $7.5 \times 7.5 \text{ mm}^2$, which is indicated by white rectangles in Figs. 2 and 4, are shown in Fig. 5. In the normal case, the 1st principal (Fig. 5(a)) strain profile shows better agreement between tMRI and 2DME than the 2nd principal strain component (Fig. 5(b)) since the lateral strain contributes more to the 2nd principal strain and thus results in their larger disagreement between two modalities. In the reperfused case, the post-infarcted (i.e., anterior and antero-septal) region experiences reduced contractility, and the normal region (i.e., posterior) compensates the systolic function for the abnormal region (i.e., anterior) with hyperkinesia, i.e., larger than normal deformation. However, this phenomenon of compensation is more pronounced in the 2DME, not in the tMRI estimates, especially the 1st principal strain component. This may explain the larger discrepancy of the principal strain in 1st component than that in 2nd component in the reperfused case. Moreover, the strains obtained from 2DME are generally higher than the equivalent tMRI values in both the normal and reperfused left ventricles (Fig. 5). Increased standard deviations in the 2DME with time and higher standard deviations of the 2DME estimates compared to those of the tMRI ones were also noted in both cases (Fig. 5).

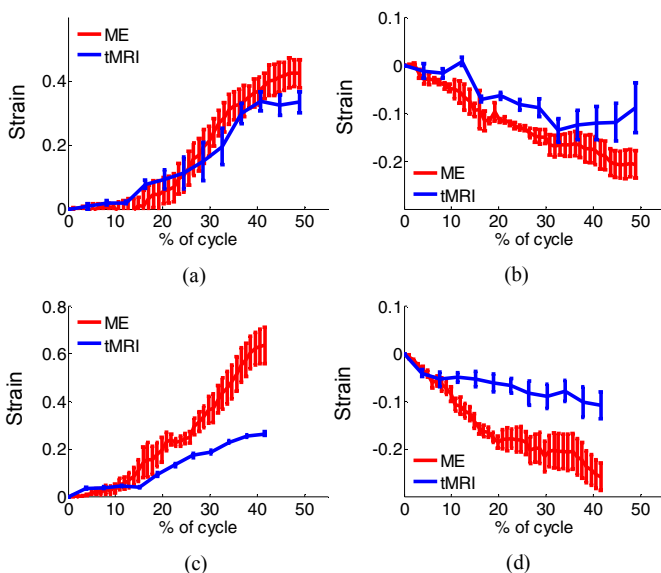


Fig. 5 Temporal principal strain profiles from 2DME and tMRI in the posterior wall region of 7.5 mm by 7.5 mm from ED to ES: (a) and (b) are the 1st and 2nd principal strain components of the normal human left ventricle, respectively; (c) and (d) are the 1st and 2nd principal strain components of the reperfused human left ventricle, respectively.

IV. DISCUSSION AND CONCLUSION

Angle-independent myocardial elastography was capable of assessing myocardial deformation with values highly comparable to those obtained with tMRI. Axial strains depicted the highest agreements between the two modalities in both normal and abnormal cases. However, the strain estimates and their transmural variations with 2DME were larger compared to those with tMRI, possibly resulting from the fact that the

ultrasound and tagged MR images were not acquired at exactly the same SA slice and that the temporal and spatial resolutions of the strain estimates in RF echocardiograms were both higher than that of tMRI. Future work will focus on exact registration of ultrasound and tagged MR images, assessment of the role of the sonographic SNR on the 2DME strain estimates and study of the tradeoff between spatial resolution and strain accuracy for precise quantification.

ACKNOWLEDGMENT

This study was supported in part by the American Heart Association (SDG 0435444T) and the National Institutes of Health (R01EB006042-01). The authors would like to thank Truman R. Brown and Christina L. Tosti for developing the MRI tagging acquisition protocol, Hamed Mojahed for acquiring the tagged MR images, Kana Fujikura and Donna Macmillan-Marotti for acquiring ultrasound data, Simon D. Fung-Kee-Fung for developing the data acquisition protocol of the ultrasound RF frames and Jianwen Luo for helpful discussion.

REFERENCES

- [1] E. E. Konofagou, J. D'hooge, and J. Ophir, *Ultrasound Med. Biol.*, vol. 28, pp. 475-482, 2002.
- [2] E. E. Konofagou, T. Harrigan, and S. Solomon, *Proc. IEEE Ultrason. Symp.*, pp. 1589-1592, 2001.
- [3] W.-N. Lee, C. M. Ingrassia, S. D. Fung-Kee-Fung, K. D. Costa, J. W. Holmes, and E. E. Konofagou, *IEEE Trans. Ultrason. Ferroelectr. Freq. Control*, 2007.
- [4] I. K. Zervantonakis, S. D. Fung-Kee-Fung, W.-N. Lee, and E. E. Konofagou, *Phys. Med. Biol.*, vol. 52, pp. 4063-4080, 2007.
- [5] S. D. Fung-Kee-Fung, W.-N. Lee, C. M. Ingrassia, K. D. Costa, and E. E. Konofagou, *Proc. IEEE Ultrason. Symp.*, pp. 516-519, 2005.
- [6] E. A. Zerhouni, D. M. Parish, W. J. Rogers, A. Yang, and E. P. Shapiro, *Radiology*, vol. 169, pp. 59-63, 1988.
- [7] L. Axel and L. Dougherty, *Radiology*, vol. 171, pp. 841-845, 1989.
- [8] Y. Notomi, P. Lysyansky, R. M. Setser, T. Shiota, Z. B. Popovic, M. G. Martin-Miklovic, J. A. Weaver, S. J. Oryszak, N. L. Greenberg, R. D. White, and J. D. Thomas, *J. Am. Coll. Cardiol.*, vol. 45, pp. 2034-2041, 2005.
- [9] T. Helle-Valle, J. Crosby, T. Edvardsen, E. Lyseggen, B. H. Amundsen, H. J. Smith, B. D. Rosen, J. A. C. Lima, H. Torp, H. Ihlen, and O. A. Smiseth, *Circulation*, vol. 112, pp. 3149-3156, 2005.
- [10] S. Wang, W.-N. Lee, J. Luo, and E. E. Konofagou, *IEEE International Ultrasonics Symposium*, New York, NY, 2007.
- [11] M. Stuber, S. E. Fischer, M. B. Scheidegger, and P. Boesiger, *Magn. Reson. Med.*, vol. 41, pp. 639-643, 1999.
- [12] E. E. Konofagou and J. Ophir, *Ultrasound Med. Biol.*, vol. 24, pp. 1183-1199, 1998.
- [13] J. Park, D. N. Metaxas, L. Axel, Q. Yuan, and A. S. Blom, *Int. J. Med. Inform.*, vol. 55, pp. 117-126, 1999.
- [14] I. Haber, D. N. Metaxas, and L. Axel, *Comput. Sci. Eng.*, vol. 2, pp. 18-30, 2000.
- [15] Z. Qian, D. N. Metaxas, and L. Axel, *Proceedings Of CVIBA Workshop, In Conjunction with ICCV, LNCS 3765*, pp. 93-102, 2005.
- [16] Z. Qian, D. N. Metaxas, and L. Axel, *Proc. of MICCAI, LNCS 4190*, pp. 636-644, 2006.
- [17] D. T. Sandwell, *Geophys. Res. Lett.*, vol. 14, pp. 139-142, 1987.
- [18] F. Kallel and J. Ophir, *Ultrason. Imaging*, vol. 19, pp. 195-208, 1997.
- [19] J. Luo and E. E. Konofagou, *IEEE Trans. Ultrason. Ferroelectr. Freq. Control*, 2007.